

An extended matched filter approach for the detection of hidden periodicities smeared by roughness

V. C. Vani[†] and S. Chatterjee^{*,#}

[†]Department of Instrumentation, Indian Institute of Science, Bangalore 560 012, India

^{*}Indian Institute of Astrophysics, Bangalore 560 034, India

From the known result that a periodic grating with a built-in roughness produces a Raman–Nath-type intensity profile, in which the peaks are smeared out by randomness, we show that an ‘extended matched filtering method’, developed by us, can reveal the hidden periodicities. The present method first anticipates the central peak, i.e. the $n = 0$ term, from a Raman–Nath intensity expression. From this residual of the intensity, the $n = \pm 1$ peaks are identified, both in terms of their location along v_x as also in terms of their amplitude. We demonstrate the effectiveness of this method by examples in which the hidden periodicities are undetectable by conventional methods and show the region of its validity.

A diffraction grating is known to have distinct peaks at periodic intervals, which get smeared out if the diffracted (or the incident) light is passed through a phase diffuser. The technique described below extracts the signal from this smeared output. Applications of this technique can be used for display devices, diffuse illuminators and for the medical imaging of certain objects.

The situation can be modelled in terms of light scattering by a rough grating surface, in the xy -plane, where the elevations $V(x, y)$ have both a periodic and a random part, given by

$$V(x, y) = a \cos(Qx) + dV(x, y), \quad (1)$$

where the random part is assumed to be a zero mean, Gaussian stationary process, such that

$$\langle dV(x, y) \rangle = 0,$$

$\langle dV(x, y) dV(x', y') \rangle = S^2 f(r)$, with $r = \sqrt{(x - x')^2 + (y - y')^2}$ in which $f(r)$ is considered to be $f(r) = \exp(-(r/l)^q)$, with $q = 1$ for the Cauchy case and $q = 2$ for the Gaussian case, l being the correlation length of the random part.

The scattering geometry is schematically described in Figure 1. The directions of the incident and scattered rays, following the convention in references 1 and 2, are expressed in polar coordinates to be $(\mathbf{q}_1, 0)$ and $(\mathbf{q}_2, \mathbf{q}_3)$, as shown in Figure 1. Further, the wave vectors of scattering are defined as,

$$\begin{aligned} v_x &= k(\sin \mathbf{q}_1 - \sin \mathbf{q}_2 \cos \mathbf{q}_3), & v_y &= -k \sin \mathbf{q}_2 \sin \mathbf{q}_3, \\ v_z &= -k(\cos \mathbf{q}_1 + \cos \mathbf{q}_2), & v_{xy}^2 &= v_x^2 + v_y^2, \end{aligned} \quad (2)$$

where $k = 2\mathbf{p}/\mathbf{l}$, \mathbf{l} being the wavelength of light.

*For correspondence. (e-mail: chat@iaps.ernet.in)

In what follows, we calculate the scattered intensity under the Kirchoff approximation, which is valid for $4\mathbf{p}r_c \cos \mathbf{q} \gg 1$, r_c being the radius of curvature of the surface. One can estimate the average radius of curvature to be $r_c \sim l^2/S$, and hence the method given below is valid only for $4\mathbf{p}(l^2/S) \cos \mathbf{q}_1 \gg 1$, and $(kr_c)^{1/3} \cos \mathbf{q}_1 \gg 1$, a case which will be maintained in the numerical cases given below.

We consider the quantity $\langle \mathbf{r} \mathbf{r}^* \rangle_0$ as the intensity of light scattered by the rough surface in the direction $(\mathbf{q}_2, \mathbf{q}_3)$ divided by the intensity of light scattered by a smooth surface in the specular direction. Following the methods indicated in ref. 3, we can show, on defining $\sqrt{g} = v_z S / \sqrt{2}$, $\sqrt{g}_1 = av_z / \sqrt{2}$, that

$$\begin{aligned} \langle \mathbf{r} \mathbf{r}^* \rangle_0 &= \{J_0^2(\sqrt{2g_1})f(v_x, v_y; g) + \sum_{n=1}^{\infty} J_n^2(\sqrt{2g_1}) \\ &\quad [f(v_x + nQ, v_y; g) + f(v_x - nQ, v_y; g)]\} \\ &B(\mathbf{q}_1, \mathbf{q}_2), \end{aligned} \quad (3)$$

where

$$\begin{aligned} f(v_x, v_y; g) &= (2\mathbf{p}/A) \\ &\int \exp(-g[1-f(r)]) J_0(v_{xy} r) r dr, \end{aligned} \quad (4)$$

$$B(\mathbf{q}_1, \mathbf{q}_2) = [F_3(\mathbf{q}_1, \mathbf{q}_2, \mathbf{q}_3)]^2 S(\mathbf{q}_1, \mathbf{q}_2), \quad (5)$$

$$\begin{aligned} F_3(\mathbf{q}_1; \mathbf{q}_2, \mathbf{q}_3) &= (1 + \cos \mathbf{q}_1 \cos \mathbf{q}_2 - \sin \mathbf{q}_1 \sin \mathbf{q}_2 \sin \mathbf{q}_3)/ \\ &(\cos \mathbf{q}_1(\cos \mathbf{q}_1 + \cos \mathbf{q}_2)), \end{aligned} \quad (6)$$

$$S(\mathbf{q}_1, \mathbf{q}_2) = S(\mathbf{q}_1)S(\mathbf{q}_2), \quad (7)$$

with

$$S(\mathbf{q}) = \exp[-(1/4) \tan \mathbf{q} \operatorname{erfc}(K \cot \mathbf{q})], \quad (8)$$

$$K^2 = (aQ)^2 + 4(S/l)^2. \quad (9)$$

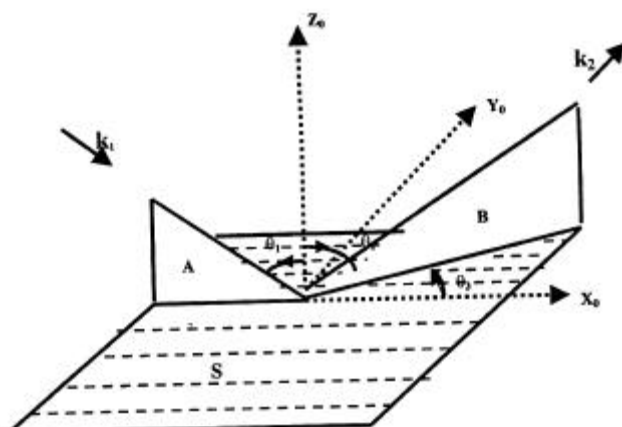


Figure 1. Orientation of the coordinate system and scattering geometry. The incident wave propagates in the direction \mathbf{k}_1 and the considered scattered wave is described by the propagation vector \mathbf{k}_2 . A is the plane of incidence and B is in the plane of scattering.

Note has to be taken of the fact that while the function $f(r)$ (expressed in italics) is defined in the xy plane, the function $f(v_x, v_y; g)$ is defined in the Fourier plane, i.e. v_x, v_y .

It is easily seen that for $\mathbf{q} = 2$, namely Gaussian correlation, one has $f(v_x, v_y; g) = (\mathbf{p}l^2/2Ag) \exp(-v_{xy}^2 r_g^2)$, with $r_g^2 = l^2/8g$, while $f(v_x, v_y; g) = [\mathbf{p}l^2/Ag^2] [1 + v_{xy}^2 c/2x]^x$ in other cases, where in the notation of papers³ $c/2x = r_0$. It is clear that for c being independent of x , in the limit of $x \rightarrow \infty$, we do get $f(v_x, v_y; g) \propto \exp(-cv_{xy}^2)$, i.e. a Gaussian profile results, showing that the choice of x can accommodate a wide range of profiles. The extended matched filter method described below, a method gives the best fit for c and x to be made in order to extract the terms J_n^2 . In what follows, we restrict ourselves to $n = 1$. This is necessitated by the fact that the parameters chosen for our numerical work are such that higher J_n^2 terms are extremely small.

The intensity expression given in eq. (3) is Raman-Nath-type, in which $B(\mathbf{q}_1, \mathbf{q}_2)$ involve certain geometrical factors as also those which contribute to shadowing effects. The factor $B(\mathbf{q}_1, \mathbf{q}_2)$ is independent of \mathbf{I} , while the factor $\{\dots\}$ in eq. (3) is strongly \mathbf{I} -dependent. Equations given in (3) and (4) show that as the width $1/r_0$ of $f(v_{xy}, g)$ increases, the zeroth-order peak is broad enough to encompass other peaks also and the detection of the periodic part becomes impossible. It was noted by Baltes and others⁴⁻¹³ that for a Gaussian correlation function the periodic part is undetectable for the randomness if $r_0/\Lambda \leq 0.33$, where $Q = 2\mathbf{p}/\Lambda$, Λ being the wavelength of the grating structure. With the help of the extended matched filter method we extract the amplitude a and the wavelength Λ of the periodic part, even in cases where $r_0/\Lambda \ll 0.33$, i.e. which do not permit identification of the periodic part by normal intensity measurements, but only by intensity interferometry¹⁴. We show that the values of a and Λ found with measurements at different wavelengths \mathbf{I} , come out to be consistently the same in the $n = 1$ case. This shows the existence of the first lobe. The second lobe is far more difficult to find, since its intensity is of the order of $(a/\mathbf{I})^4$ and may be extremely low in the case under study. For an accurate detection of the grating structure, one can perform experiments at different \mathbf{I} s and show that the amplitude of the $n = \pm 1$ lobe follows the $(a/\mathbf{I})^2$ dependence on \mathbf{I} . For the present, we study the accuracy to which the $n = \pm 1$ lobe and the wave vector Q of the grating can be found. In doing so we have studied the accuracy with which the $n = \pm 1$ lobes and Q can be found at different wavelengths \mathbf{I} of light that is used, where the change in \mathbf{I} alters the value of the quantity (r_0/Λ) , detectability being worse as (r_0/Λ) becomes smaller.

Considering that $\sqrt{g_1} \ll 1$, the amplitudes of the successive n th peaks fall as $(\sqrt{g_1})^{2n}$, while the width of the peaks vary as $\Delta v_x \sim r_0^{-1}$. The separation of the peaks being $\Delta v_x = Q$, the central $n = 0$ peak can submerge all the higher order peaks for $\Delta v_x \gg \Delta v_x = Q$. Here, the extended matched

filtering method uses the same principle as given earlier by us^{15,16}, but follows a more accurate method to arrive at the best filter. As before, this method too envisages the shape $f(v_x, g)$ of the central peak and separates it out from the total intensity profile. In this way it tries to identify the $n = \pm 1$ peaks whose shape must match with that of the $n = 0$ peak that has been eliminated out.

We begin by assuming (this is the shape of the central peak which must be the same for all other peaks too) that

$$f(v_x) = f_a(v_x) \equiv [1 + (c'/2y)v_x^2]^y, \quad (10)$$

and note that on defining

$$Z(v_x) = [\langle \mathbf{r}^*(v_x) \mathbf{r}(v_x) \rangle / \langle \mathbf{r}^*(0) \mathbf{r}(0) \rangle] - f_a(v_x), \quad (11)$$

$$\mathbf{c}(v_x) = Z(v_x)/Z_{\max}, \quad (12)$$

we have from eqs (3), (11) and (12),

$$\mathbf{c}(v_x) = (N_0 + N_1 + N_2)/(D_0 + D_1 - D_2), \quad (13)$$

where we have defined,

$$\begin{aligned} N_0 &= J_0^2[f(v_x) - f_a(v_x)], \\ N_1 &= J_1^2[f(v_x + Q) + f(v_x - Q) - 2f_a(v_x)f(Q)], \\ N_2 &= J_2^2[f(v_x + 2Q) + f(v_x - 2Q) - 2f_a(v_x)f(2Q)], \\ D_0 &= J_0^2[f(Q) - f_a(Q^*)], \\ D_1 &= J_1^2[f(Q^* + Q) + f(Q - Q^*) - 2f_a(Q^*)f(Q)], \\ D_2 &= J_2^2[f(Q^* + 2Q) + f(Q^* - 2Q) - 2f_a(Q^*)f(2Q)], \end{aligned} \quad (14)$$

and Q^* is the wave vector at which $Z(v_x)$ has a maxima.

It is clear that when our assumed $f_a(v_x)$ is very close to the actual $f(v_x)$, the terms N_0 and D_0 become negligible and the terms N_1 show prominent peaks at $v_x = \pm Q^* \approx \pm Q$, while these lobes at $v_x \approx \pm Q^*$ should match with the chosen $f_a(v_x)$. To quantitatively select the best match, we note that if the terms N_0 and D_0 be negligible (because of the match $f(v_x) \approx f_a(v_x)$), we must have $\mathbf{c}(v_x) - \mathbf{c}_a(v_x)$ to be extremely small where $\mathbf{c}_a(v_x)$ is defined as,

$$\mathbf{c}_a(v_x) = \mathbf{c}_{aN}(v_x)/\mathbf{c}_{aD}(v_x), \quad (15)$$

where

$$\mathbf{c}_{aN}(v_x) = [f_a(v_x + Q^*) + f_a(v_x - Q^*) - 2f_a(v_x)f_a(Q^*)], \quad (16)$$

$$\mathbf{c}_{aD}(v_x) = [f_a(Q^* + Q^*) + f_a(Q^* - Q^*) - 2f_a(Q^*)f_a(Q^*)], \quad (17)$$

and the matched filtering is effected by defining an estimator

$$\Delta^2 = \int_0^{Q^*} |\mathbf{c}_a(v_x) - \mathbf{c}(v_x)|^2 dv_x. \quad (18)$$

We select the filter by choosing the c' , and y to be the one which gives Δ^2 to be the minimum. Note must be taken of the fact that while $\mathbf{c}(v_x)$ is a quantity which is found from the experimental data, $\mathbf{c}_a(v_x)$ is a quantity that

is given by our hypothesis, while Δ^2 gives a least square estimate of the deviation of data from the hypothesis under consideration. The main aim in the extended matched filtering method is to anticipate $f(v_x)$ first, such that the shape of $f_a(v_x)$ describing the $f(v_x)$ must also match the shapes of the side lobes at $n = \pm 1$ to be found by searching for the minimum of Δ^2 . The Δ^2 defined above is different from that given by Chatterjee and Vani^{15,16}. On redefining Δ^2 as given here, we note that the identification of the matched filter is considerably improved.

Identification of the matched filter enables us to 'detect', through a least square fit, the parameters for the rough part of the surface. To find those for the periodic part, we use eq. (11) to give (on defining $f'(v_x) = \partial f / \partial v_x$),

$$f'_a(Q^* + Q) + f'_a(Q - Q^*) - 2f_a(Q)f'_a(Q^*) = \\ -(J_1/J_0)^2 [f'(Q^* + 2Q) - f'(Q^* - 2Q)], \quad (19)$$

$$Z_{\max}J_0^2 - [f_a(0) + f_a(2Q^*) - 2f_a^2(Q^*) - 2f_a(Q^*)Z_{\max}] \\ J_1^2 - [f_a(3Q^*) + f_a(Q^*) - 2f_a(2Q^*)f_a(Q^*) \\ - 2f_a(Q^*)Z_{\max}]J_2^2 = 0, \quad (20)$$

the typical results from which are given next.

In the numerical implementation of our scheme, we have chosen a case in which $r_0/I \leq 0.33$, i.e. the periodic part is to be undetectable by ordinary intensity measurements, except by intensity interferometry. The numbers chosen are $\Lambda = 6.25$ micron, $s = 0.15$ micron, $l = 5$ microns and $q = 1.0$, being the same as in our earlier works¹⁵⁻¹⁷. In making these choices, we have taken a situation where the Kirchoff conditions (i) $4pr_c \cos q_1 \gg I$ and (ii) $(kr_c/2)^{1/3} \cos q_1 \gg 1$ are maintained. In this case $(4pr_c \cos q_1/I) \sim 4000 \gg 1$, while $(kr_c/2)^{1/3} \sim 8$, so that condition (ii) is also valid as long as $\cos q_1 \gg 0.125$. It is clear that r_0 is I -dependent in this case, but (r_0/Λ) still lies in the undetectable limit in every case that we present here. It should be further noted that the detectability limit $r_0/I = 0.33$ is true for the case of the correlation between the randomness, i.e. in the $q = 2$ case for the exponent in the correlation function for the randomness. In the case chosen here we have $q = 1$, and the

detectability is not possible even for $r_0/I = 0.40$, by studying the intensity profile, up to which we have checked. For higher I s an idea about Q can be obtained if one tries to observe structures in the differentiated signals a_1 and a_2 , being defined as: $a_1 = [(\partial \langle \mathbf{r}^* \mathbf{r} \rangle_0 / \partial v_x) / \langle \mathbf{r}^* \mathbf{r} \rangle_0]$ and $a_2 = [(\partial^2 \langle \mathbf{r}^* \mathbf{r} \rangle_0 / \partial v_x^2) / \langle \mathbf{r}^* \mathbf{r} \rangle_0]$. This structure is, however, not seen in the case of $I = 5700 \text{ \AA}$ that we have discussed below. However, the parameters are detectable to a fair degree of accuracy in regions far below the detectability cut-off (Table 1) while the conventional methods would not have allowed such a detectability.

In our earlier work we had effected matched filtering by choosing $c_a = f_a(v_x - Q^*)$ and obtained satisfactory values when $I = 6328 \text{ \AA}$. The extended matched filter presented here describes $c(v_x)$ much more accurately than the function $c_a(v_x)$ that has been described in our earlier work. The present method is thus more accurate than the matched filter described earlier. This is unmistakably seen when we note that the minima in Δ^2 becomes sharper in the present extended matched filtering than what was seen in the earlier version. This makes the best filter to be more easily discernible, than was in the method presented earlier. It is also to be noted that Δ^2 is more sensitive to c' than to y , i.e. is extremely robust up to the second derivative or to the curvature of $f(v_x)$. As the values in Table 1 show, y appears to be the same, i.e. 1.55 (correct one being 1.50) independent of I , as it should be. The values of Λ and a are also independent of I – within limits of permissible error – as is physically demanded, taking into account that in both the cases we are measuring sub wavelength distances, since $(a/I) \sim 0.051$, $(\Lambda/I) \sim 0.05-0.10$. This improved detectability is related to the central point in matched filtering that the $f_a(v_x)$ selected must give a satisfactory match to $f(v_x)$. From the parameters of randomness used in our numerical simulations, the quantity r_0^2 is calculable and is expected to follow $(I^2 r_0) = \text{constant}$. Correct identification of the matched filter would demand that that $(c'/2y r_0^2) = 1$ in every case. This is indeed found to be so, the ratio defined on the left side differing from unity by 10% in the worst case that has been encountered here. This shows that the method is quite satisfactory in

Table 1. Numerical calculation for the hidden periodic part. Intensity simulations are made for a rough grating with $\Lambda = 6.25$ microns, i.e. $Q = 1.005 \times 10^4 \text{ cm}^{-1}$, $s = 1.5 \times 10^{-5} \text{ cm}$, $l = 5 \times 10^{-4} \text{ cm}$. While the wavelength I of light is different, in every case the amplitude a of the periodic part is adjusted so that $(a/I) = 0.052$, thus keeping the argument of the Bessel function terms at the $n = \pm 1$ peaks to be 0.65 so that the corresponding parameter $(J_1/J_0)^2 = 0.0070$ in every case. Intensity profile does not show any peak other than the central one. Numerical values of Q and a as found from the matched filtering are shown to give satisfactory results

Wavelength (\AA)	r_0 (micron)	Q (calculated) (micron $^{-1}$)	a/I (calculated)	r_0/Λ	Error in a (%)	Error in Q (%)
10000	2.527	0.994	0.052	0.4044	0.37	- 1.09
7500	1.422	0.995	0.054	0.2275	4.62	- 0.99
6000	0.910	1.001	0.048	0.1456	7.7	- 0.40
5000	0.632	1.040	0.040	0.1011	24.7	+ 3.48

finding the factor $f_a(v_x)$. Indeed as (r_0/Λ) reduces, the errors in finding c' and y do contribute to large errors in finding Q^* and Z_{\max} , due to the smallness of (a/I) and hence the detectability suffers immensely. The limit for detectability by this method appears, in a preliminary estimate, to be $(r_0/I) \approx 0.12$, far lower than the limit put by Baltes and others for detection by usual intensity measurements.

The effectiveness of our method can be understood from the following argument. In the discussions on detectability, Baltes and others considered whether the $n = 0$ and the $n = 1$ peaks could be seen separately. This means they were tackling the distinguishability of two peaks whose amplitudes differ by a factor of $(a/I)^2$ and which are separated by $\Delta v_x = Q$. In our extended matched filtering, once the $n = 0$ peak is filtered out we are to distinguish the two comparable peaks at $n = \pm 1$ but separated by a larger $\Delta v_x = 2Q^*$. The latter, according to the Rayleigh criterion or the Sparrow criterion^{18,19}, allows distinguishability of the peaks for much lower values of r_0 . In the results presented here the errors are indeed tolerable, but the errors in Q^* and a reach as high as 30%, when $(r_0/\Lambda) \sim 0.065$. This communication unmistakably establishes the extended matched filtering as a promising new tool for detection of hidden periodicities, purely from intensity data. Numerical experiments choosing various sets of parameters are under way and we further plan to advance this scheme by making a statistical error analysis and issues of goodness-of-fit.

13. Jauch, K. M., Baltes, H. P. and Glass, A. S., Measurement of coherence of radiation from diffusively illuminated beam splitters. *Proc. Soc. Photo-Opt. Instrum. Eng.*, 1982, **369**, 687–690.
14. Dainty, J. C. and Newman, D., Detection of gratings hidden by diffusers using photon correlation techniques. *Opt. Lett.*, 1983, **8**, 608–610.
15. Chatterjee, S. and Vani, V. C., Scattering of light by periodic structure with randomness. *Bull. Astron. Soc. India*, 2002, **30**, 835–836.
16. Chatterjee, S. and Vani, V. C., On the scattering of light by a periodic structure in the presence of randomness II. On the detection of weak periodicities. *J. Mod. Opt.*, 2003, **50**, 833–845.
17. Vani, V. C. and Chatterjee, S., An extended matched filtering method to detect periodicities in a rough grating for extremely large roughness. *Bull. Astron. Soc. India*, 2003 (communicated).
18. Barakat, R., Application of apodization to increase two point resolution by the Sparrow criterion I. Coherent illumination. *J. Opt. Soc. Am.*, 1962, **52**, 276–283.
19. Barakat, R. and Levin, E., Application of apodization to increase two point resolution by the Sparrow criterion. II Incoherent illumination. *J. Opt. Soc. Am.*, 1963, **53**, 274–282.

Received 23 May 2003; revised accepted 1 September 2003

Arabian Sea mini warm pool during May 2000

**K. V. Sanilkumar*, P. V. Hareesh Kumar,
Jossia Joseph and J. K. Panigrahi**

Naval Physical and Oceanographic Laboratory, Thrikkakkara,
Kochi 682 021, India

Anomalously warmer waters, viz. the Arabian Sea mini warm pool were reported in the southeastern Arabian Sea, which is believed to drive the onset vortex of the southwest monsoon. To understand the characteristics of this mini warm pool, an experiment was conducted on-board INS Sagardhwani during the middle of May 2000. Analysis of the oceanographic data revealed the existence of a mini warm pool with temperature in excess of 30.25°C along 9°N between 68 and 75.5°E during the pre-onset period of the southwest monsoon. This mini warm pool coincided with the regions of low salinity (35.2 PSU) layer and its intensity inversely correlated with the depth of the highly stable ($E > 2000 \times 10^{-8} \text{ m}^{-1}$) layer. At the core (73.5°E, 9°N) of the mini warm pool, surface temperature was 31.2°C and sea surface salinity was less than 34.6 PSU. This core was found restricted to the upper 5 m water column following the thickness of low-salinity pocket and the

1. Beckman, P. and Spizzichino, A., *The Scattering of Electromagnetic Waves from Random Surfaces*, Pergamon Press, London, 1963.
2. Beckman, P., Scattering of light by rough surfaces. In *Progress in Optics* (ed. Wolf, E.), North Holland, 1967, vol. 6, p. 53.
3. Chatterjee, S., On the scattering of light by a periodic structure in presence of randomness. *Indian J. Phys. B*, 2000, **74**, 363–366.
4. Baltes, H. P., Fewerda, H. A., Glass, A. S. and Steinle, B., Retrieval of structural information from far zone intensity and coherence of scattered radiation. *Opt. Acta*, 1981, **28**, 11–28.
5. Baltes, H. P. and Ferwerda, H. A., Inverse problems and coherence. *IEEE Trans. Antennas Propag.*, 1981, **AP-29**, 405–406.
6. Baltes, H. P., Glass, A. S. and Jauch, K. M., Multiplexing of coherence by beam splitters. *Opt. Acta*, 1981, **28**, 873–876.
7. Baltes, H. P. and Jauch, K. M., Multiple version of the van Zittert – Zernike theorem. *J. Opt. Soc. Am.*, 1981, **71**, 1434–1439.
8. Glass, A. S. and Baltes, H. P., The significance of far zone coherence for sources or scatterers with hidden periodicity. *Opt. Acta*, 1982, **29**, 169–185.
9. Glass, A. S., Baltes, H. P. and Jauch, K. M., The detection of hidden diffractors by coherence measurements. *Proc. Soc. Photo-Opt. Instrum. Eng.*, 1982, **369**, 681–686.
10. Jauch, K. M. and Baltes, H. P., Coherence of radiation scattered by gratings covered by a diffuser. Experimental evidence. *Opt. Acta*, 1981, **28**, 1013–1015.
11. Glass, A. S., The significance of image reversal in the detection of hidden diffractors by interferometry. *Opt. Acta*, 1982, **29**, 575–583.
12. Jauch, K. M. and Baltes, H. P., Reversing wave front interferometry of radiation from a diffusively illuminated phase grating. *Opt. Lett.*, 1982, **7**, 127–129.